20-T, 120-cm-I.R. Target Magnet with Large Axial Gaps at z = 3, 9 &15 m

Bob Weggel, Magnet Optimization Research Engineering, LLC
1/19/2012

This report revises and extends one entitled "20-T, 120-cm-I.R. Target Magnet with Layer-Wound Resistive Magnet," of 5/11/2011, which designed target magnets optimized by a computer program with major upgrades to its predictions of superconductor current density, coil stresses & strains, and cost-optimization parameters. Fig. 1 shows the field-and-temperature dependence of the non-copper current density in the Nb_3Sn in the strands of the superconducting cable, as generated by Eq. (1):

$$j(B,T) \cong \frac{46{,}630}{B}(1-t^{1.247})^2\, b^{0.437}(1-b)^{1.727} \ \text{[A/mm}^2\text{]}. \qquad (1)$$

The magnetic flux density B is in teslas; t and b are, respectively, the normalized temperature T/T_c and normalized magnetic flux density $B/B_c(T)$, where T_c and B_c are the critical temperature and critical field defined respectively by $j(B=0, T_c) = 0$ and $j(B_c|T) = 0$. Eq. (1) resembles that of "A general scaling relation for the critical current density in Nb_3Sn," by A Godecke, B ten Haken, H H J ten Kate and D C Larbalestier (2006 Supercond. Sci. Technol. **19** R100 doi: 10.1088/0953-2048/19/10/R02), but gives a much closer fit to the $j(B,T)$ data for Nb_3Sn of the ITER barrel magnet tabulated on page 645 of *Case Studies in Superconducting Magnets*, by Y. Iwasa. Fig. 2 plots the parameter $B_c = 20.8 - 1.27\,T - 0.0234\,T^2$ needed by Eq. (1). Data points from which to generate the curve fit of Fig. 2 came from T_c = 18.2 K and the $j(B|T)$ curves of Fig. 3a-b, which give $B_c(T) =$ 28.8 T at 1.8 K, 24.5 T at 4.2 K and 16.1 T at 10 K.

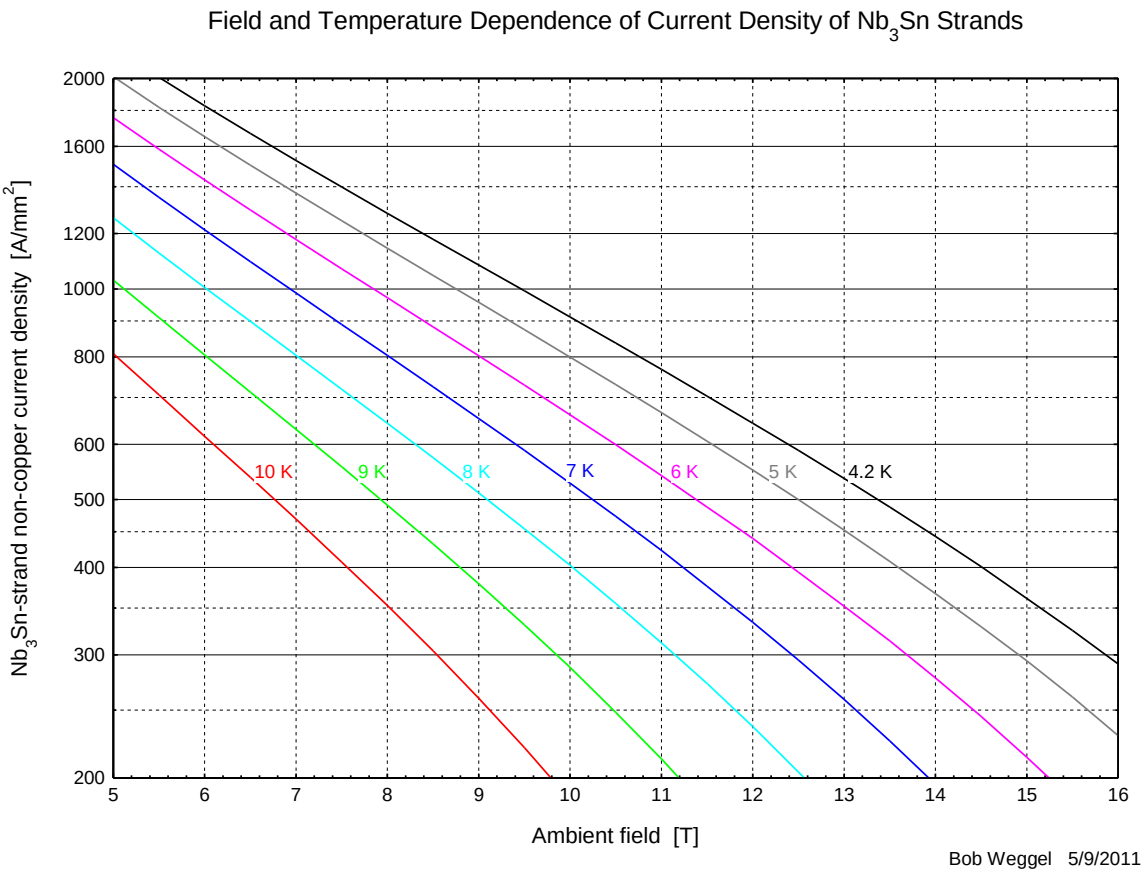

Fig. 1: Non-copper current density vs. field and temperature for Nb_3Sn strands of ITER barrel magnet.

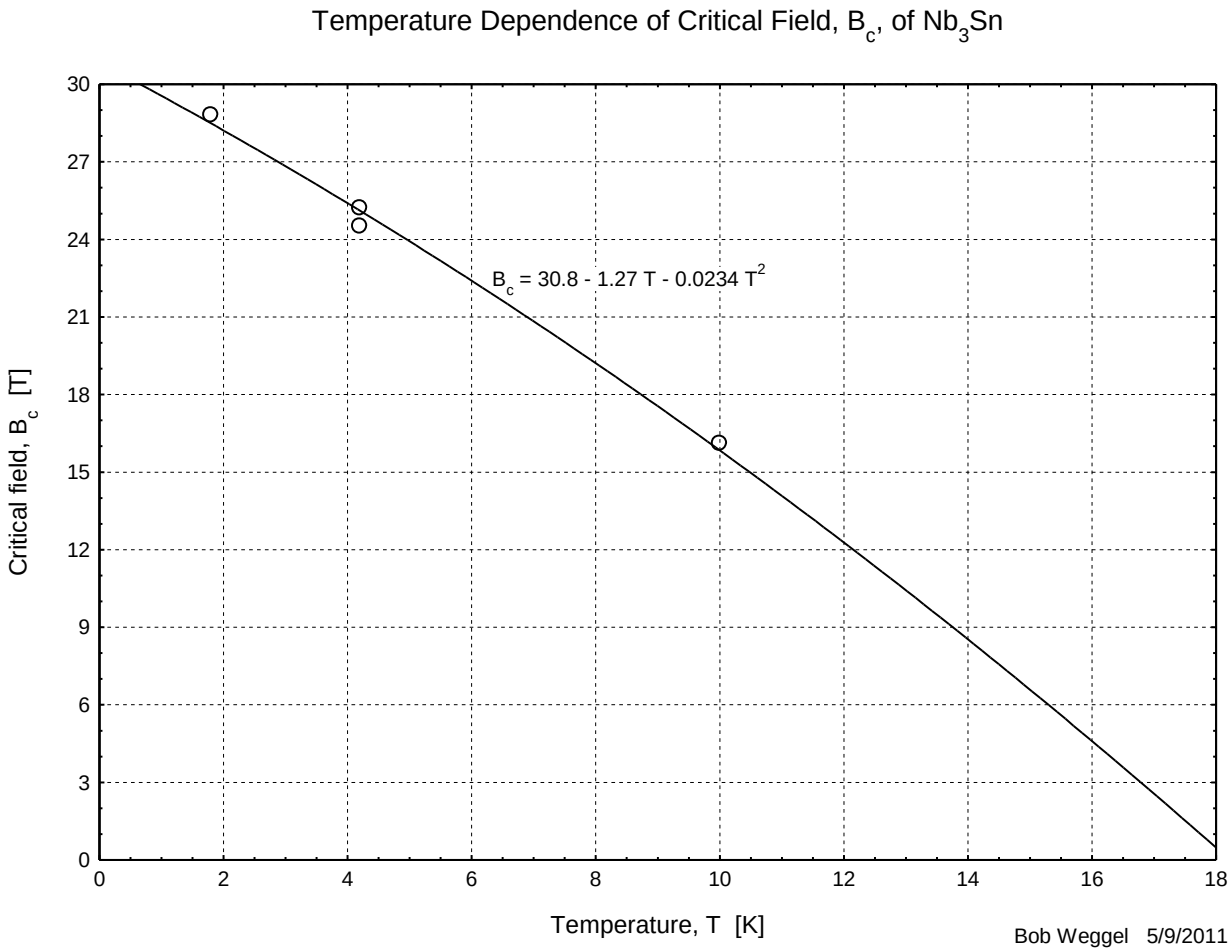

Fig. 2: Curve fit of data generated by Fig. 3a-b. $B_c(T) = 20.8 - 1.27\,T - 0.0234\,T^2$ teslas.

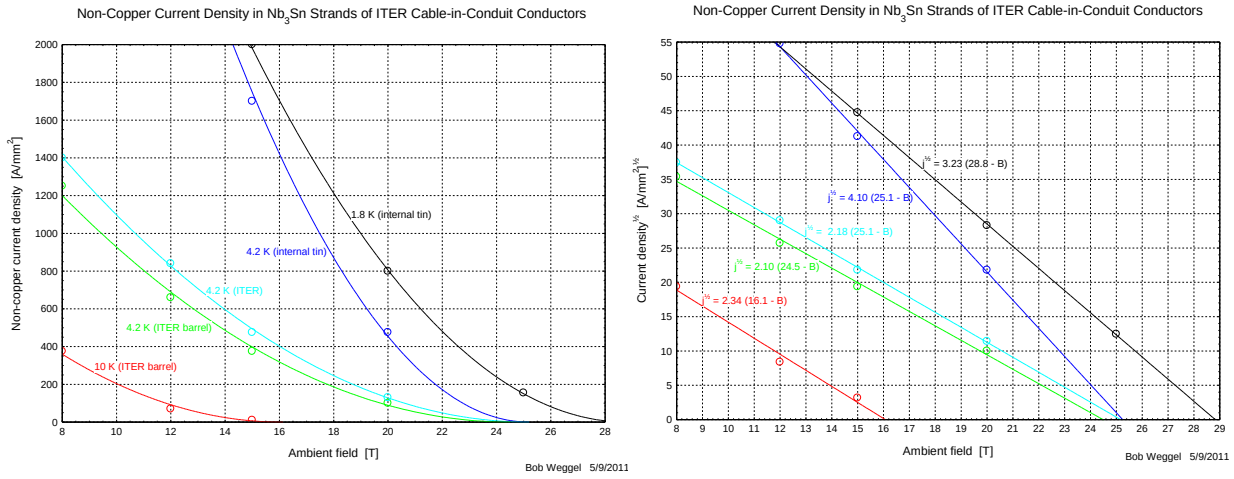

Fig. 3a-b: Curve fits of $j(B|T)$ by $j(B)\sim(B_c - B)^2$. Left: $j(B|T)$. Right: $\sqrt{j(B|T)}$. For ITER barrel conductor, extrapolation of the red curve to $j = 0$ gives B_c = 16.1 T at 10 K; extrapolation of the green curve gives B_c= 24.5 T at 4.2 K. For internal-tin conductor, B_c = 25.1 T at 4.2 K (blue curve) and 28.8 T at 1.8 K (black curve).

To predict the maximum stress in each coil (always at the inner radius, if the turns are bonded sufficiently to prevent them from separating radially), the computer program uses Eq. (5.35b) on p. 124 of *Solenoid Magnet Design* by Montgomery & Weggel or, equivalently, Eq. (3.77b) on p. 101 of *Case Studies in Superconducting Magnets*. The coil is of inner radius a_1, outer radius a_2, current density j, bore field B_1 and external field B_2, and is of isotropic material of Poisson's ratio ν = 0.3. The predicted stress is:

$$\sigma_{max} = j\,\frac{(7a_1^2 + 14a_1a_2 + 85a_2^2)(B_1 + B_2) + 14(a_1^2B_1 + a_2^2B_2)}{120(a_1 + a_2)} \quad .$$

Fig. 4 presents the results. Note that for a radially-thin coil (radius ratio $\alpha \equiv a_2/a_1 = 1+\Delta$), the peak stress is $\sigma_{max} = j_1\, a_1 \langle B \rangle$, where $\langle B \rangle = (B_1+B_2)/2$, the average field in the windings. In a coil of radius ratio α = 1.6 and field ratio β = 0 (appropriate for the most-upstream superconducting coil of a 20-T target magnet), the normalized stress $\sigma^* \equiv \sigma_{max} / (j_1\, a_1\, B_1)$ is 0.85. If α = 2.8 and β = 0.7 (appropriate for a pancake-wound resistive magnet of O.R. = 50 cm and I.R. = 18 cm) the normalized stress σ* is 2.85. The actual coil is layer-wound, radially partitioned and banded with stainless steel to reduce this stress.

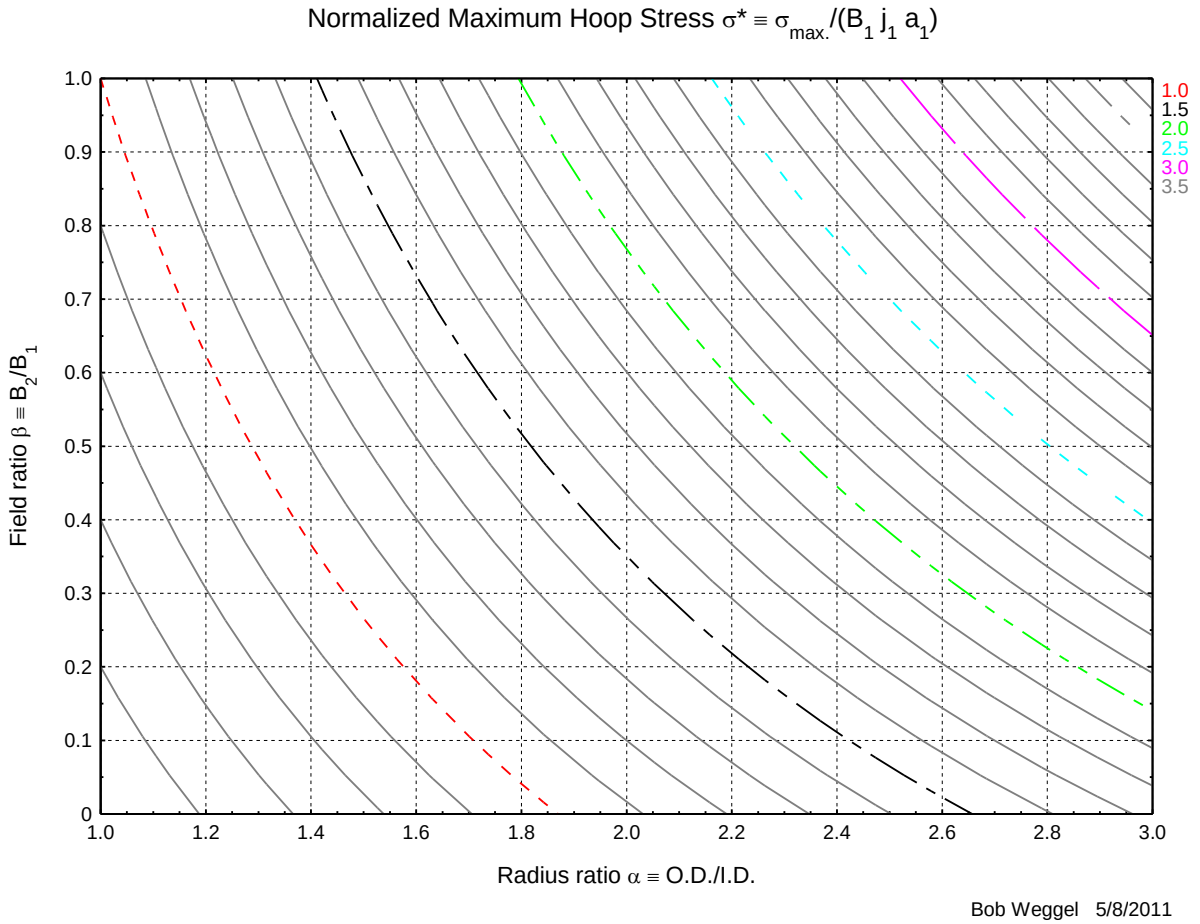

Fig. 4: Normalized maximum hoop stress $\sigma^* \equiv \sigma_{max.}/(B_1\, j_1\, a_1)$ vs. radius ratio $\alpha \equiv$ O.R./I.R. & field ratio $\beta \equiv B_2/B_1$.

Fig. 5a-d, generated by a finite-element-method program, confirms that the magnet-optimization program does indeed generate designs in which the peak strain in every coil is at most ~0.4%, which should be acceptable for the resistive-coil copper and stainless steel and for the superconducting-coil Nb_3Sn, copper stabilizer and stainless steel conduit, the only member counted on to bear load.

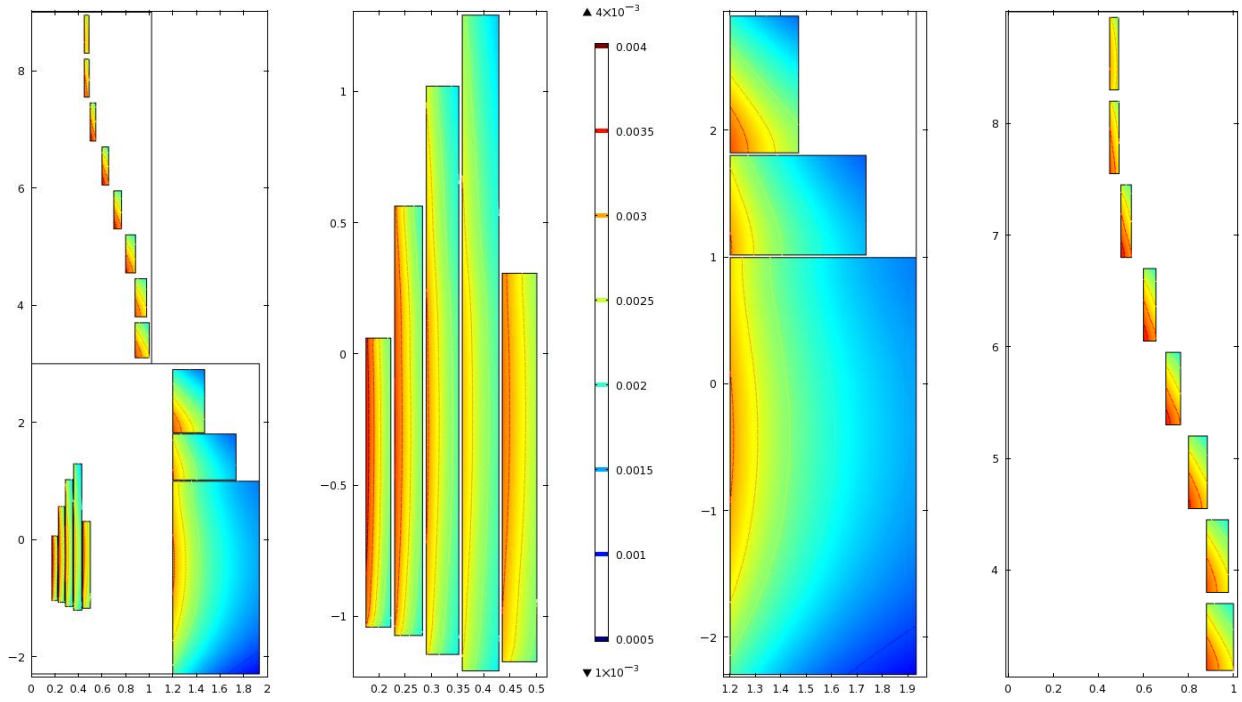

Fig. 5a-d: Hoop strain ε_{hoop} (color & contour lines) of Target Magnet "IDS120h". Left: Resistive magnet & SC coils upstream of 9 m. Left center: Resistive coils only. Right center: Upstream SC coils. Right: Downstream SC coils.

To accommodate support structure and the many vessel walls, radiation shields and vacuum spaces of cryostats, the design IDS120h should have much larger axial gaps between its cryostats, each of which should be not much longer than 6 meters if the vessel containing its shielding is not to sag excessively with only cantilever support. Fig. 6 shows the cross section of coils in a magnet with intercoil axial gaps of: a) 50 cm at z = 3 m; b) 35 cm at z = 9 m and; c) 27.5 cm at z = 15 m. The optimization program, which minimizes a weighted sum of resistive-magnet power consumption, superconductor cost, and accuracy of on-axis field profile, is able to make the actual field profile match the desired one very closely.

The magnet of Fig. 7, with coil lengths optimized (not done for the Fig. 6 coils downstream of z = 3 m) has much wider intercoil axial gaps: 115 cm, 78 cm and 55 cm. Each gap is 1/3 the sum of the outer radii of the coils which flank it, a guess of the space needed between adjacent coils not in the same cryostat. Despite the large axial gaps and fewer (12 instead of 19) superconducting coils upstream of 15 meters, the magnet has field quality comparable to that of Fig. 6.

Fig. 8 and Table I describe a magnet of comparable gap widths (112 cm, 79 cm and 60 cm) and field quality but only ten superconducting coils upstream of 15 m. Like the previous magnets, its resistive magnet has five nested two-layer coils of radiation-resistant MgO-insulated hollow conductor and upstream superconducting coils of 120-cm inner radius. Its total stored energy is 3.3 GJ; its on-axis field profile from z = −75 cm to 0 is parabolic, 20.2 T at its center and 19.5 T at its ends, a field inhomogeneity of 0.73T, or 3.6%, peak-to-peak.

Table I lists a multitude of magnet parameters. The resistive magnet employs 6.7 metric tons of Japanese-Hadron-Facility hollow conductor. The innermost coil uses 0.345 tons (108 meters) of 18.0-mm square O.D. (Conductor parameters not shown are: overall O.D., including insulation and non-current-carrying copper sheath, is 23.8 mm; cooling hole is 10 mm square.) Coils further out scale this to as much as 25.8 mm square O.D.—i.e., twice the cross section and therefore half the current density. Supporting each coil is a tube or wrap 1.5 mm to 3.0 mm thick of 700 MPa design stress and 200 GPa

Young's modulus. The magnet has 602 turns; the field contribution is 5.3 T at 11.6 MW: 940 volts at 12.4 kA. The maximum temperature rise in the conductor is 80°C with 50 liters/second of water at a pressure drop of 40 atmospheres and three hydraulic paths per layer in the inner coil and four paths per layer in each of the other coils.

The most-upstream superconducting coil has an O.R. of 196 cm, a length of 3.7 meters, a weight of 170 metric tons, and is 9.3% Nb_3Sn, 52% stainless steel and 15% each of copper and helium, leaving 8% for insulation. Coil #15 of Table I is 1.0% superconductor (modeled as Nb_3Sn), 5.4% stainless steel (again of 700 MPa design stress and 200 GPa Young's modulus) and 37.5% each of copper and helium, leaving 19% for insulation.

Fig. 9 shows that the on-axis field quality of the magnet remains comparable to that of Figs. 6 and 7.

Fig. 10 shows that the maximum hoop strain in every coil is the design value of 700 MPa/200 GPa = 0.35%. To achieve this required several iterations between the analytic program that optimizes coil dimensions and the FEM program that computes accurately the magnetic field off-axis, not merely on-axis, and also the Lorentz forces, stresses and strains.

Figs. 10 and 11 plot the axial and radial components, respectively, of the magnetic field. To limit the number of curves to eleven, for clarity, each graph—$B_z(z|r)$ and $B_r(z|r)$—plots curves only for radii that are integer multiples of 20 cm. The data points for each curve are a subset of a field map "IDS120i_B.txt" that covers the range z = −500 cm to +1480 cm in increments of 20 cm, and r = 0 to 200 cm in increments of 5 cm. The mesh could be much finer, if desirable for MARS predictions of power-deposition density.

The field map employs a computer program with exquisite accuracy even within the conductor volume, achieved by computing the field from the actual volumetric current density, rather than modeling each coil by a number of current-sheet solenoids. The current-sheet-solenoid model computes neither B_r nor B_z accurately within the windings of coils. 1) At a distance Δz beyond the end of any current-sheet solenoid of axial length Z the radial component of field B_r is proportional to $\ln(Z/\Delta z)$, which approaches infinity as Δz approaches zero. 2) The axial component of field B_z is discontinuous, by an amount $\mu_0 NI$, on opposite sides of a current-sheet solenoid carrying a current per unit length of NI amperes per meter. Even with a large number of current-sheet solenoids to model each coil, these discontinuities will be large—e.g., an error in B_z of ~±½ tesla in a 15-tesla coil modeled by 15 current-sheet solenoids. Modeling each coil with a distributed current density, rather than a set of current-sheet solenoids, completely eliminates these errors.

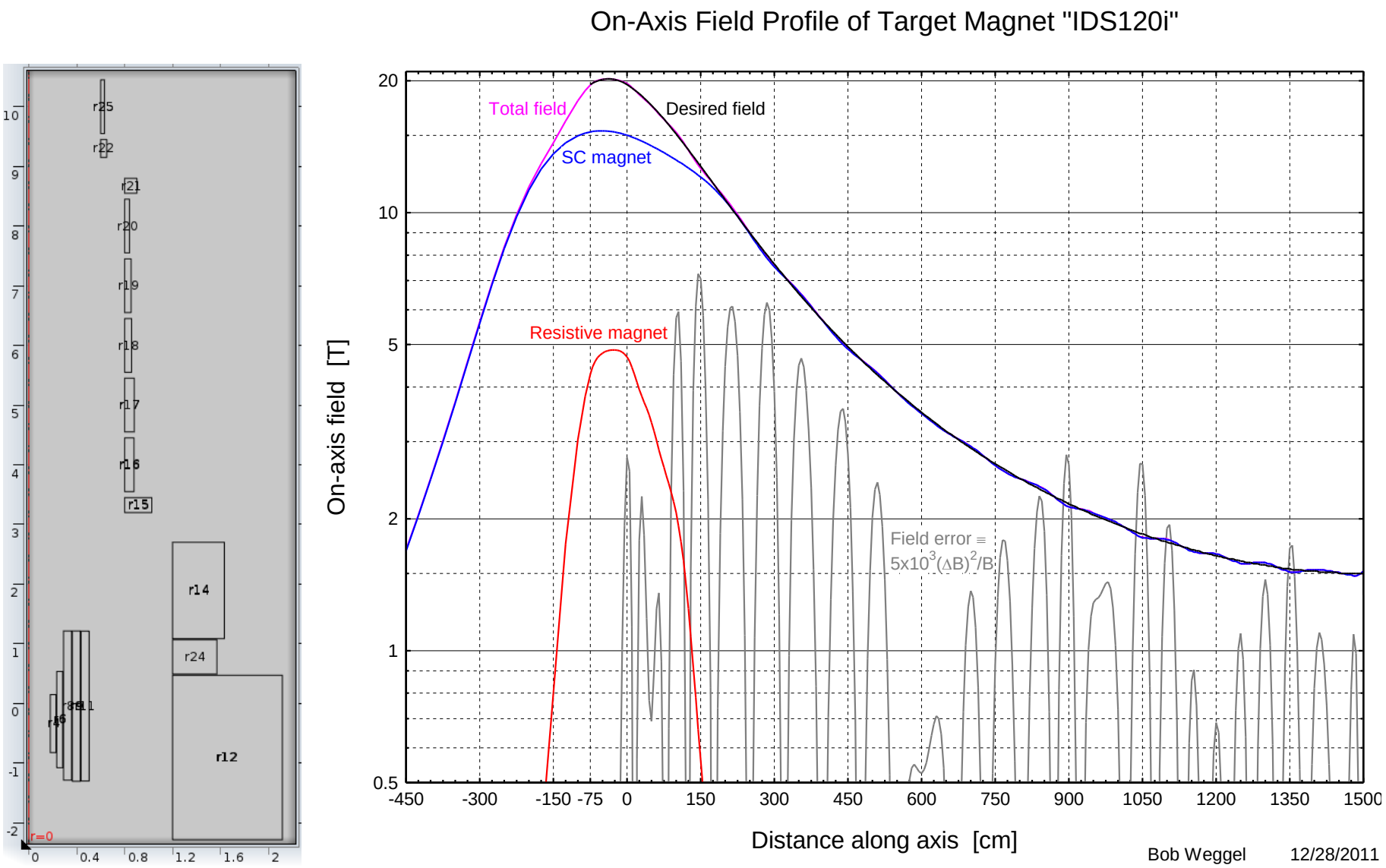

Fig. 6a-b: Resistive & upstream twelve superconducting coils of Magnet IDS120i3m with intercoil axial gap of 50 cm flanking z = 3 meters and axial gap of 35 cm flanking z = 9 meters. Left: Coil cross sections. Right: On-axis field profiles of superconducting, resistive and combined magnet.

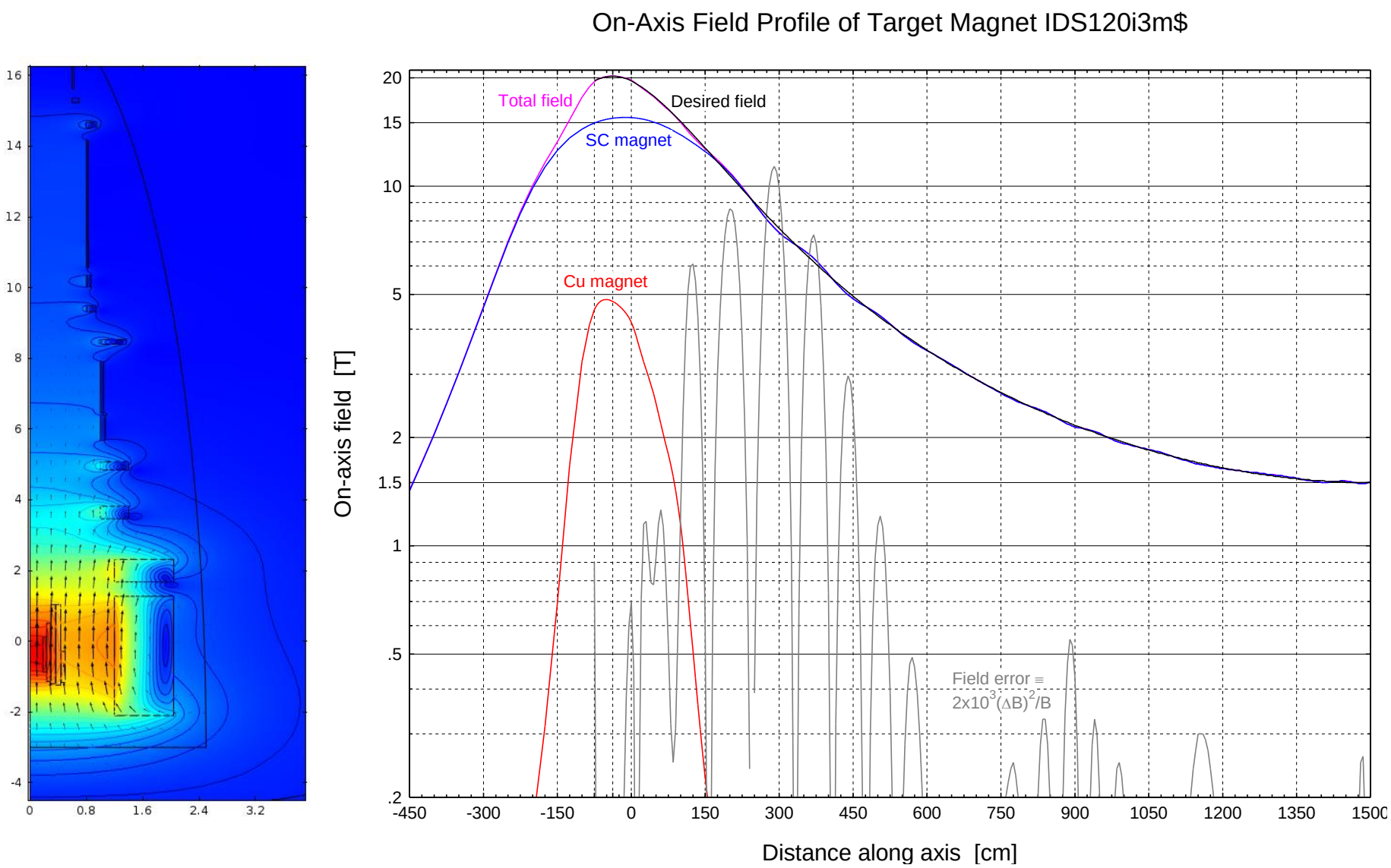

Fig. 7a-b: Resistive & superconducting (SC) coils of Target Magnet IDS120i3m$. Intercoil axial gaps at z = 3 m, 9 m & 15 m of 115 cm, 78 cm & 55 cm; each gap width is 1/3 the sum of the outer radii of the coils that flank the gap. O.D.'s of SC coils constrained, to decrease cryostat O.D.'s. Quarter ellipse is boundary between medium & coarse FEM mesh. Left: Coil cross-sections & field magnitude (color & contours) & direction (arrows). Right: On-axis field profiles of SC, resistive & combined magnet.

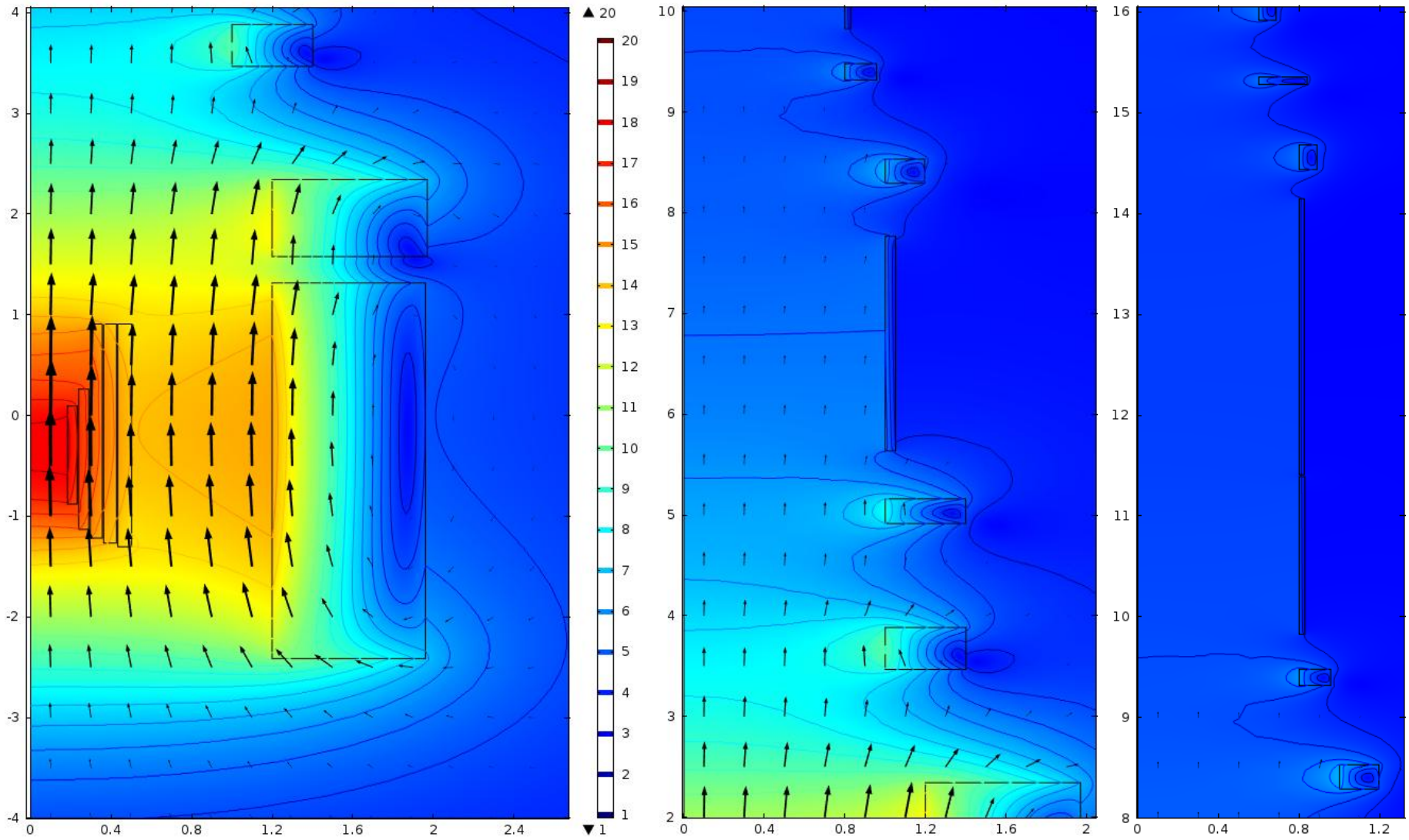

Fig. 8a-c: Coil cross-sections & field magnitude (color & contours) & direction (arrows) of resistive and superconducting coils of Target Magnet IDS120i3m^. Intercoil axial gaps at z = 3 meters, 9 meters & 15 meters of 112 cm, 79 cm & 60 cm; each gap width is 1/3 the sum of the outer radii of the coils that flank the gap. Outer diameters of superconducting coils constrained, to decrease cryostat outer diameters. Left: −4 m < z < +4 m. Center: 2 m < z < 10 m. Right: 8 m < z < 16 m.

Table I: Parameters of Target Magnet IDS120i3m^

	System:	**12.39**	kA	0.1	meters ΔL_{elec}		1.724	$\mu\Omega$cm at 20 °C		7.0	nΩcm/deg		10.0	°C T_0	40.0	atmospheres ΔP		0.10	m ΔL_{hy}
	Coil designation		Units	sum	1	2	3	4	5	6	7	8	9	10	11	12	13	14	15
	O.D. of square hollow conductor		cm		1.800	**1.902**	**2.235**	**2.418**	**2.578**										
	SSt shell estimated thickness		cm		**0.250**	**0.295**	**0.187**	**0.167**	**0.151**										
	Current density $j\lambda_{coil}$		kA/cm^2		2.187	1.959	1.418	1.212	1.066	**1.928**	**2.255**	**3.196**	**3.666**	**4.121**	**4.337**	**4.470**	**4.620**	**4.685**	**4.682**
	Coil length		cm		**97.4**	**139.3**	**212.5**	**217.5**	**221.2**	**373.2**	**76.5**	**41.6**	**24.5**	**213.0**	**24.1**	**16.2**	**156.3**	**273.7**	**24.5**
	Gap between coils		cm							**26.1**	112.4	103.2	**47.6**	**52.6**	78.6	34.6	**2.0**	**28.9**	59.9
	Upstream end		cm		**-87.9**	**-113.1**	**-121.7**	-126.7	-130.4	-241.5	157.8	346.7	491.5	563.6	829.2	931.9	982.7	1141.0	1443.6
	Downstream end		cm		9.5	26.2	90.8	90.8	90.8	131.7	234.3	388.3	516.0	776.5	853.3	948.1	1139.0	1414.7	1468.1
	Turns/layer; ends [cm]		slope		40.92	55.40	71.90	68.02	64.90										
	Min. I.R. [cm]	0.17	-0.10		18.36	21.70	29.68	29.68											
	Inner radius		cm		18.36	23.87	29.69	36.29	43.35	120.0	120.0	100.0	100.0	100.0	100.0	80.0	80.0	80.0	80.0
	Layers of hollow conductor				2.00	2.00	2.00	2.00	2.00										
	Radial depth		cm		4.76	5.03	5.91	6.39	6.82	**76.13**	**77.02**	**40.16**	**40.01**	**5.14**	**19.59**	**15.69**	**2.90**	**2.58**	**8.88**
	Outer radius		cm		23.12	28.90	35.60	42.68	50.17	196.13	197.02	140.16	140.01	105.14	119.59	95.69	82.90	82.58	88.88
	Volume, inc. SSt shell		m^3	39.40	0.064	0.124	0.267	0.355	0.454	28.22	5.87	1.26	0.74	0.71	0.33	0.14	0.23	0.36	0.12
	Magnetic moment		MA-m^2	631	0.14	0.30	0.60	0.83	1.11	438.3	107.0	24.39	16.40	14.91	7.78	2.76	4.37	6.88	2.28
	Conductor length		m	1312	108	185	297	339	383										
	Maximum on-axis field		T		20.21	19.02	17.88	16.88	15.96	15.11	12.28	6.67	4.47	3.75	2.40	2.10	1.96	1.71	1.52
	Est .peak isotropic stress		MPa		103.0	107.8	90.4	87.2	85.1	299.6	286.3	206.1	118.1	101.9	62.9	56.8	42.6	33.2	31.8
	Strain correction factor		0.35		1.247	1.272	1.098	1.050	1.011	1.219	1.209	1.139	1.470	1.086	1.333	1.160	1.056	1.101	1.182
	SC current density		[A/mm^2							208	414	1254	1971	2330	3383	3738	3940	4348	4714
	SC γ, MPa & fraction	6.00								0.093	0.054	0.025	0.019	0.018	0.013	0.012	0.012	0.011	0.010
	Cu γ, MPa & fraction	8.95	100	0	0.550	0.550	0.550	0.550	0.550	0.154	0.180	0.256	0.293	0.330	0.347	0.358	0.370	0.375	0.375
	SSt γ, MPa & fraction	7.80	700	700	0.050	0.055	0.031	0.025	0.022	0.522	0.495	0.335	0.248	0.158	0.120	0.0941	0.0643	0.0522	0.0537
	SSt cm & SC M$	30	$90.2		0.250	0.295	0.187	0.167	0.151	$78.4	$9.60	$0.96	$0.412	$0.374	$0.125	$0.050	$0.082	$0.117	$0.034
	Coil tons	M$/m^3	6.70	220.4	0.345	0.667	1.416	1.877	2.393	169.3	34.02	6.18	3.37	2.95	1.32	0.55	0.88	1.36	0.43
	M$@$200/kg	0.40	$2.68	$88.1	3	4	4	4	4	paths/layer									
	Wrap pressure σ_r	M$/ton	MPa		7.53	7.11	3.67	2.73	2.11										
	Magnet voltage		V	938	122	190	216	206	202										
	Magnet MW or MA-m		11.62	83.44	1.52	2.36	2.68	2.56	2.50	54.41	13.24	4.03	2.71	2.91	1.41	0.63	1.07	1.69	0.54
2.0	x10^7 s Max. ΔT_{bulk} [°C]		$7.82	56.8	59.5	67.9	63.8	52.9	46.5										
	Total hot spot ΔT		°C		72.9	80.0	72.3	60.0	52.7										
	True average total T		°C		52.5	55.4	50.0	43.2	39.1										

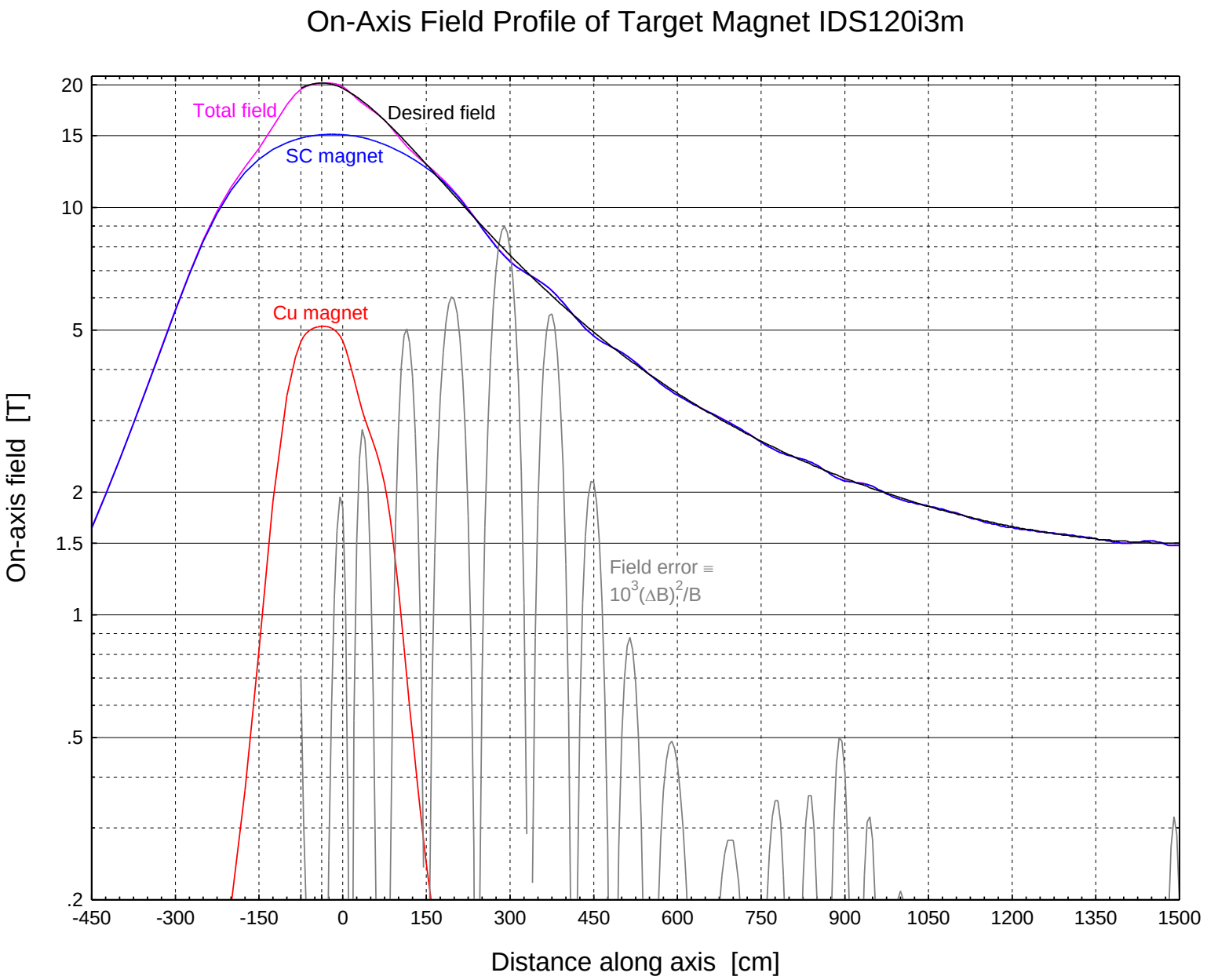

Fig. 9: On-axis field profiles of superconducting, resistive and combined magnet of Fig. 8 and Table I.

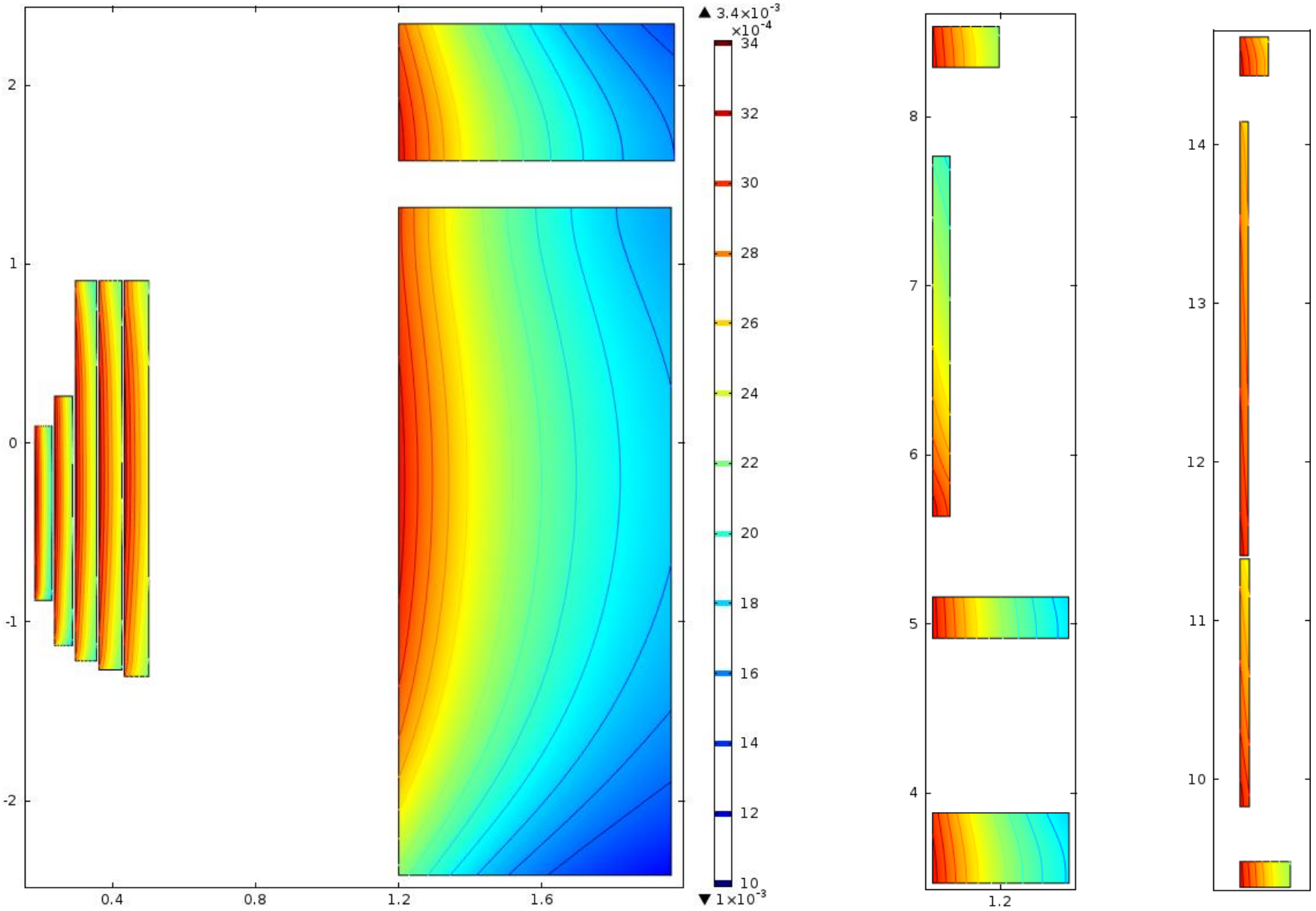

Fig. 10a-c: Maximum hoop strain σ_{hoop} is 0.35% in every coil IDS120i^. Left: z = −3 m to +3 m (upstream module). Center: 3 m to 9 m. Right: 9 m to 15 m.

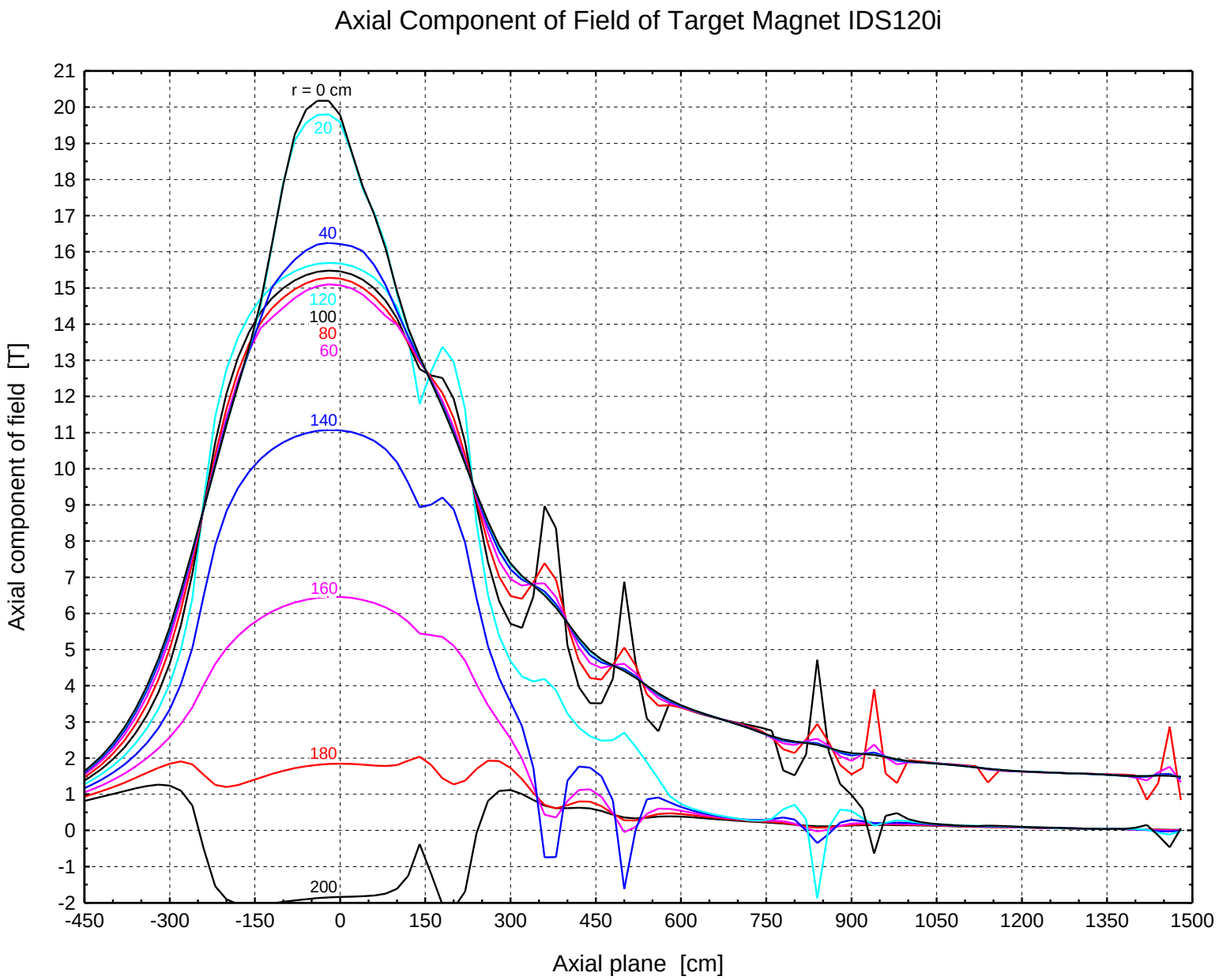

Fig. 11: Axial component of field of Target Magnet IDS120i of Figs. 8-10 and table I.

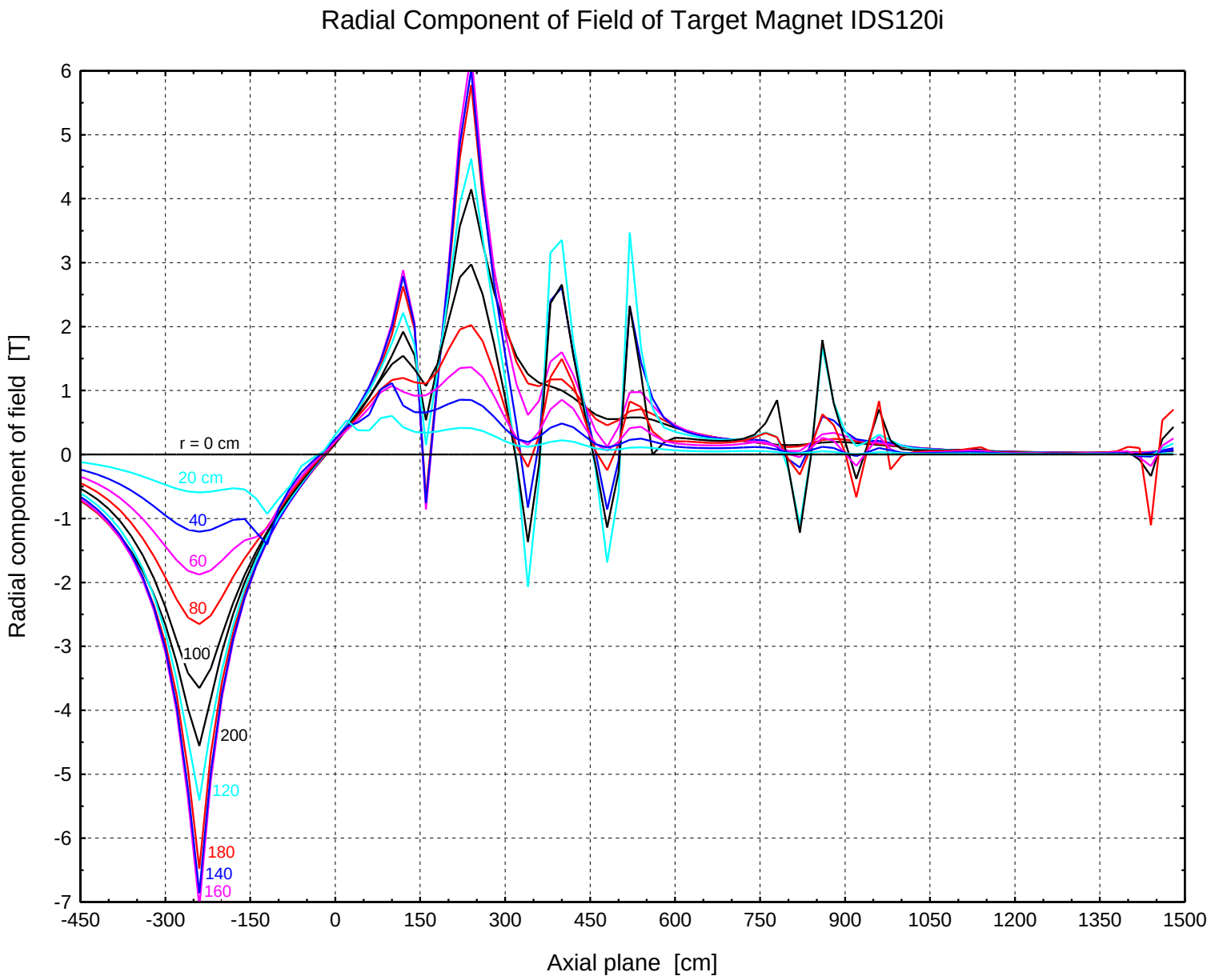

Fig. 12: Radial component of field of Target Magnet IDS120i of Figs. 8-10 and Table I.